Human Molecular Genetics, 2015, 1–16

doi: 10.1093/hmg/ddu735
Advance Access Publication Date: 30 December 2014
Original Article

ORIGINAL ARTICLE

Toll-like receptor 4 ablation in mdx mice reveals innate immunity as a therapeutic target in Duchenne muscular dystrophy

Christian Giordano[1], Kamalika Mojumdar[1], Feng Liang[1], Christian Lemaire[1], Tong Li[1], John Richardson[2], Maziar Divangahi[1], Salman Qureshi[1,3] and Basil J. Petrof[1,*]

[1]Meakins-Christie Laboratories and Respiratory Division, McGill University Health Centre, [2]Department of Pathology, McGill University and [3]Department of Critical Care, McGill University Health Centre, Montreal, Quebec, Canada

*To whom correspondence should be addressed at: Meakins-Christie Laboratories, 3626 St. Urbain Street, Montreal, QC H2X 2P2, Canada. Tel: +1 5143983864; Fax: +1 5143987483; Email: basil.petrof@mcgill.ca

Abstract

Toll-like receptor 4 (TLR4) recognizes specific structural motifs associated with microbial pathogens and also responds to certain endogenous host molecules associated with tissue damage. In Duchenne muscular dystrophy (DMD), inflammation plays an important role in determining the ultimate fate of dystrophic muscle fibers. In this study, we used TLR4-deficient dystrophic mdx mice to assess the role of TLR4 in the pathogenesis of DMD. TLR4 expression was increased and showed enhanced activation following agonist stimulation in mdx diaphragm muscle. Genetic ablation of TLR4 led to significantly increased muscle force generation in dystrophic diaphragm muscle, which was associated with improved histopathology including decreased fibrosis, as well as reduced pro-inflammatory gene expression and macrophage infiltration. TLR4 ablation in mdx mice also altered the phenotype of muscle macrophages by inducing a shift toward a more anti-inflammatory ($iNOS^{neg}$ $CD206^{pos}$) profile. *In vitro* experiments confirmed that lack of TLR4 is sufficient to influence macrophage activation status in response to classical polarizing stimuli such as IFN-gamma and IL-4. Finally, treatment of dystrophic mice with glycyrrhizin, an inhibitor of the endogenous TLR4 ligand, high mobility group box (HMGB1), also pointed to involvement of the HMGB1–TLR4 axis in promoting dystrophic diaphragm pathology. Taken together, our findings reveal TLR4 and the innate immune system as important players in the pathophysiology of DMD. Accordingly, targeting either TLR4 or its endogenous ligands may provide a new therapeutic strategy to slow disease progression.

Introduction

Duchenne muscular dystrophy (DMD) is the most common X-linked lethal disorder in humans, with an incidence of ~1 in 3500 male births. Because the disease involves the diaphragm and other respiratory muscles, most patients will die of respiratory failure unless supported by mechanical ventilation. DMD is caused by defects in dystrophin, a protein which confers important structural (e.g. mechanical reinforcement of sarcolemma) and signaling (e.g. regulation of intracellular calcium and nitric oxide synthase) properties to skeletal muscle (1). The absence of dystrophin is associated with skeletal muscle fiber death, which occurs principally through necrosis. In DMD patients, corticosteroids are the only pharmacological agents approved for slowing disease progression, albeit with very limited

Received: August 28, 2014. **Revised:** November 27, 2014. **Accepted:** December 22, 2014

success and considerable side effects (2). The mdx mouse, which harbors a premature termination codon in the dystrophin gene, is the most commonly used animal model of DMD (3).

It is clear that dystrophin deficiency is necessary, but not sufficient on its own, to fully account for the pathophysiology of DMD. In this regard, the critical role played by inflammation has been demonstrated by eliminating macrophages and other inflammatory cell types in mdx mice (4–6), as well as through strategies to inhibit key mediators of inflammation such as NF-kB (7) and TNF-α (8). Thus current evidence suggests that the repeated episodes of muscle fiber necrosis as well as the subsequent fibrotic response of DMD skeletal muscle are driven to a large extent by complex interactions between dystrophin deficiency and the host immune response (9).

The innate immune system has evolved to identify invading pathogens via a set of germline-encoded receptors, termed pattern recognition receptors (PRRs), which are capable of recognizing structural motifs common to many different microorganisms (10). It is increasingly evident that these PRRs also recognize and respond to various endogenous tissue molecules found in pathological conditions (11,12). In general, endogenous ligands for PRRs are molecules which accumulate in non-physiologic sites or amounts or have been altered from their native state, as a result of tissue damage. They have thus been referred to as 'endogenous danger signals', 'alarmins' or 'damage associated molecular patterns' (DAMPs).

One of the largest classes of PRRs is the Toll-like receptor (TLR) family, whose members differ with regard to the microbial components which they detect as well as their subcellular distribution (10). The best studied of these is probably Toll-like receptor 4 (TLR4), which is localized to the cell surface where it recognizes bacterial lipopolysaccharide (LPS). The list of non-microbial DAMPs recognized by TLR4 has been steadily accumulating in the literature, which includes components of the extracellular matrix, heat shock proteins and other molecules associated with cell death or tissue inflammation (11,12). Among the DAMPs recognized by TLR4 is high mobility group box 1 (HMGB1), a highly conserved protein that normally performs homeostatic functions in the nucleus (13), but which can be released from cells during cell death through active or passive mechanisms (13–17).

The therapeutic benefits of inhibiting either TLR4 or its endogenous ligands have been demonstrated in disease models involving various organs (18–21). In this study, we hypothesized that endogenous DAMPs, including but not necessarily limited to HMGB1, could signal through TLR4 to stimulate innate immunity and thereby play a direct role in driving disease progression in the mdx mouse model of DMD.

Results

TLR4 upregulation and hyperresponsiveness in mdx mice

To ascertain whether exaggerated TLR4 signaling could be involved in DMD pathophysiology, we first assessed TLR4 mRNA expression levels in the diaphragm. As compared with WT mice, an approximate 3-fold increase of TLR4 mRNA was observed in the mdx group (Fig. 1A). We next evaluated whether dystrophic muscles are more responsive to TLR4 stimulation *in vivo*, by injecting WT and mdx mice with the exogenous TLR4 agonist LPS (25 mg/kg i.p.). Diaphragm muscles were removed 1.5 and 3 h later for western blotting (Fig. 1B) to assess IkBα phosphorylation (p-IkBα) and total IkBα degradation, which were used as an index of NF-kB activation. In response to LPS administration, the mdx muscles showed greater levels of p-IkBα (Fig. 1C and D), more sustained degradation of total IkBα (Fig. 1E and F) and a higher p-IkBα/total IkBα ratio (Fig. 1G and H). Taken together, these alterations in the magnitude and timing of NF-kB activation following TLR4 agonist exposure are consistent with an augmented sensitivity to TLR4 pathway stimulation in the dystrophic group.

TLR4 ablation alleviates muscular dystrophy progression in mdx mice

To determine the specific role of TLR4 in DMD pathogenesis, we generated TLR4-deficient mdx mice (mdx-TLR4–/–). The impact of TLR4 ablation on diaphragm force generation in dystrophic mice was determined at 6 and 12 weeks of age. These age groups were selected because the younger age represents a more intense inflammatory stage, whereas in the older group inflammation is less prominent and muscles are considered to be in a more reparative/fibrotic phase. At all muscle stimulation frequencies studied, mdx diaphragms were profoundly weak compared with their age-matched WT counterparts (Figs. 2A and B). Although muscle strength was not entirely restored to WT levels, the diaphragms of mdx-TLR4–/– mice demonstrated significant improvements in maximal force-generating capacity, which amounted to average increases of 49 and 67% over mdx values at 6 weeks (Fig. 2C) and 12 weeks (Fig. 2D) of age, respectively.

We next evaluated whether the improved contractile function of mdx-TLR4–/– muscles was accompanied by changes in the characteristic histopathological features of dystrophic muscle. A classical hallmark of DMD is the presence of regenerated muscle fibers with centrally located nuclei, which are almost entirely absent in undamaged muscle and can thus be used as a marker for prior cycles of necrosis-regeneration (22). As compared with mdx, the mdx-TLR4–/– mice diaphragms exhibited a 59% decrease in the proportion of centrally nucleated fibers at 6 weeks (Fig. 3A) and a 40% reduction at 12 weeks (Fig. 3B). The limb muscle (tibialis anterior) of mdx-TLR4–/– mice showed comparable reductions in centrally nucleated fibers in the two age groups (Supplementary Material, Fig. S1A and B). Values for fiber size (minimum Feret's diameter) in centrally nucleated fibers (Fig. 3C and D) as well as in the totality of fibers sampled within the muscle (Fig. 3E and F) were larger in the mdx-TLR4–/– group at 12 weeks, suggesting more effective reconstitution of muscle fiber size during the regenerative phase of the disease. A size distribution analysis for all fibers (Fig. 3G and H) confirmed an overall shift toward larger fiber sizes in mdx-TLR4–/– diaphragms. In addition, the mean variance coefficient, an index of the myofiber size heterogeneity which is characteristically increased in dystrophic muscles, was significantly reduced in mdx-TLR4–/– muscles in both age groups (Fig. 3I and J).

Muscle fibrosis, an important element of muscular dystrophy progression, was also assessed in mdx-TLR4–/– mice. Two different methods were employed to evaluate muscle collagen content: stereological quantification of modified Gomori trichrome staining (Fig. 4A and B), and biochemical measurements of hydroxyproline content (Fig. 4C and D). Both approaches revealed the expected progression of diaphragm fibrosis from 6 to 12 weeks of age in mdx mice. The severity of fibrosis was significantly alleviated in mdx-TLR4–/– mice at both ages, as indicated by decreases in hydroxyproline content of 33% (at 6 weeks) and 48% (at 12 weeks) in comparison to age-matched mdx counterparts. The level of fibrosis was also decreased in the tibialis anterior muscles of mdx-TLR4–/– mice (Supplementary Material,

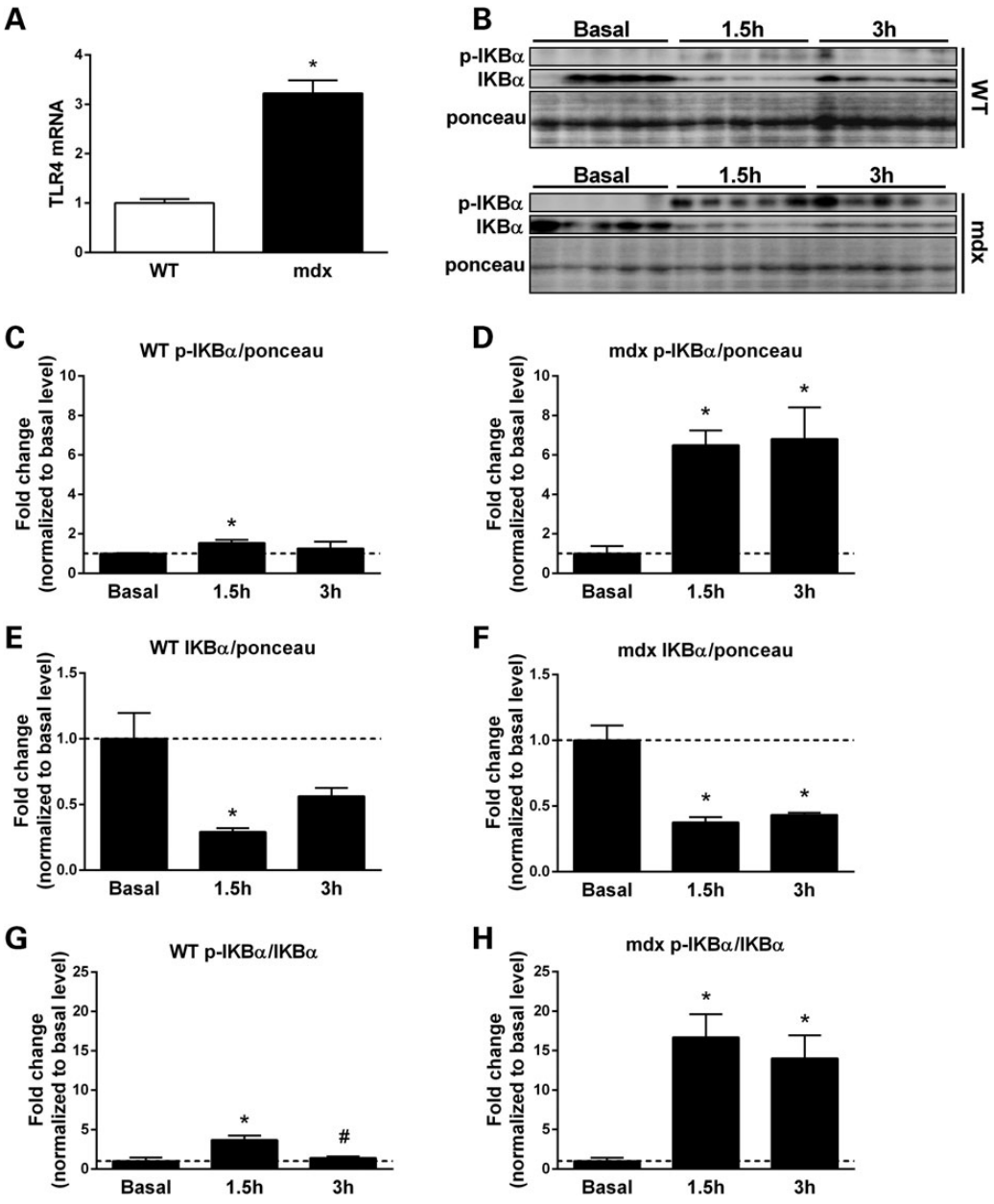

Figure 1. TLR4 pathway upregulation in mdx mice. (**A**) Real-time polymerase chain reaction (PCR) quantification of TLR4 in WT and mdx diaphragm. (**B**) Western blot images of phosphorylated (p-IKBα) and total (IKBα) levels of IkBα proteins in WT (upper panel) and mdx (lower panel) diaphragms, either untreated (basal level = dashed line) or stimulated for the indicated duration with 25 mg/kg LPS i.p. (**C, D**) Densitometric quantification of p-IkBα in WT and mdx. (**E, F**) Densitometric quantification of total IkBα in WT and mdx. (**G, H**) Densitometric quantification of p-IkBα/IkBα ratio in WT and mdx. $N = 5$ mice per group; $^{*}P < 0.01$ between WT and mdx (by *t*-test for panel A); $^{*}P < 0.05$ compared with basal value (by ANOVA for panels C–H).

Fig. S1C and D). Finally, we evaluated abnormal sarcolemmal permeability, another typical feature of muscles lacking dystrophin, by staining dystrophic myofibers for circulating IgG. In comparison to the mdx group, diaphragm myofibers of mdx-TLR4–/– mice exhibited significantly reduced IgG staining at 12 weeks of age (Fig. 4E and F), suggesting a reduction in damaged fibers with excessive membrane leakiness.

Muscle inflammation is reduced in mdx mice lacking TLR4

Macrophages are a key component of innate immunity regulated by TLR4 and constitute by far the predominant inflammatory cell type within dystrophic muscles (23). Immunostaining of macrophages (F4/80 antibody) was compared between mdx and mdx-TLR4–/– mice on randomly selected muscle sections (Fig. 5A). The total muscle surface area exhibiting F4/80 positivity was significantly lower in mdx-TLR4–/– mice, amounting to decreases of ~70% compared with mdx mice at 6 weeks of age (Fig. 5B). Moreover, using a real-time quantitative polymerase chain reaction (PCR) array analysis of 75 genes related to TLRs and their associated signaling pathways (see Supplementary Material, Table S1), we identified a significant downregulation of numerous genes involved in pro-inflammatory signaling in the diaphragms of mdx-TLR4–/– mice compared with the mdx group at 6 weeks (Fig. 5C). Interestingly, in many instances the basal

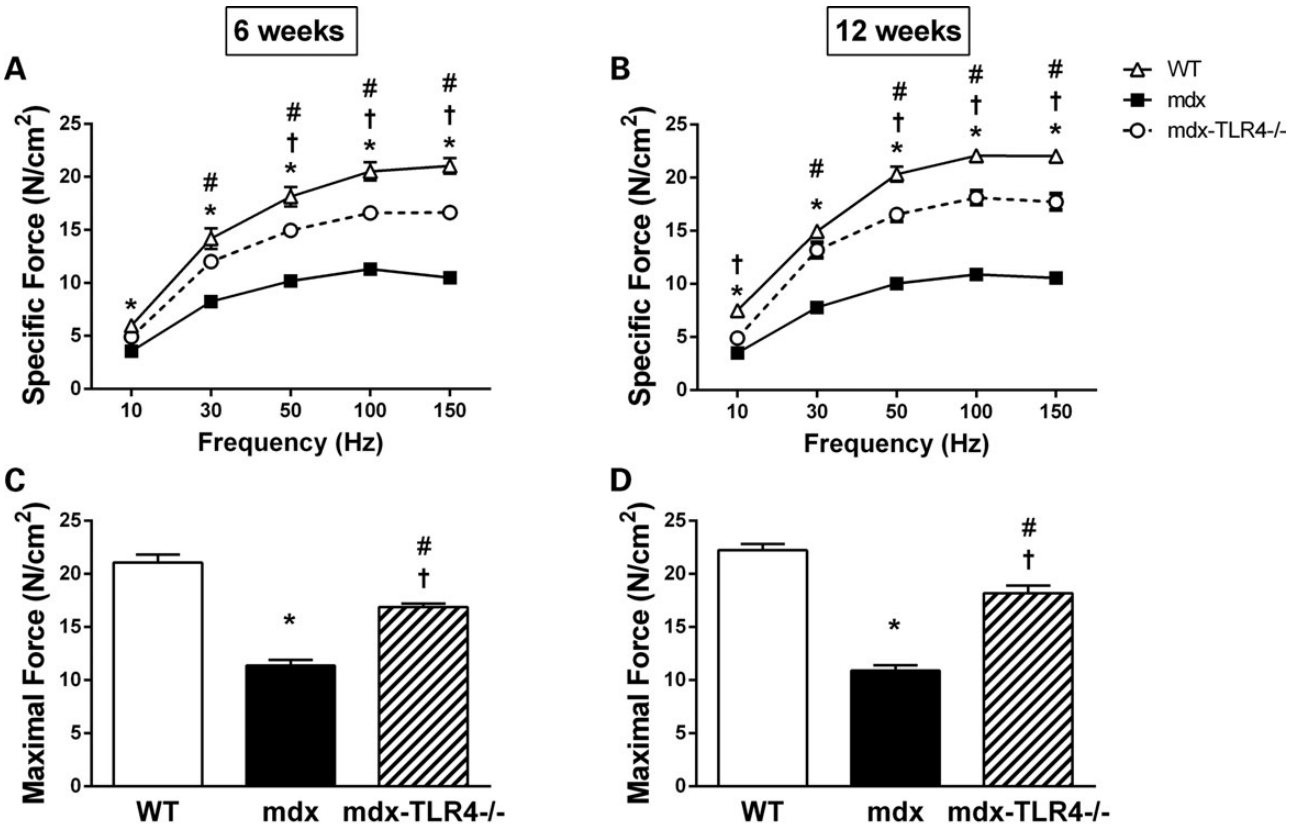

Figure 2. Genetic ablation of TLR4 improves contractile function of dystrophic diaphragm. Force–frequency curves obtained during electrical stimulation of diaphragms from WT, mdx and mdx-TLR4–/– mice at (**A**) 6 weeks of age and (**B**) 12 weeks of age. Quantification of maximum force-generating capacity of diaphragms from the three mouse strains at (**C**) 6 and (**D**) 12 weeks is also shown. $N = 8$ mice per group; $^{*}P < 0.05$ between WT and mdx; $^{\#}P < 0.05$ between mdx and mdx-TLR4–/–; $^{\dagger}P < 0.05$ between WT and mdx-TLR4–/– (by ANOVA).

expression levels of these genes in mdx mice were not substantially altered relative to WT levels, yet their mRNA levels were significantly diminished in the mdx-TLR4–/– group. The affected genes included regulators of NF-kB activation (e.g. IKKα, IKKβ and IkBα), downstream targets of NF-kB (e.g. IL-1α, IL-1R, TNFα, TNFα-R, IL-12 and IL-6R), protein kinases (e.g. MEKK1, MKK3 and JNK2), members of the TLR signaling pathway (e.g. TICAM-1, TIRAP and Tollip) and mediators involved in regulating cell death (e.g. FADD). Finally, although the basal level of macrophage infiltration in mdx diaphragms was lower at 12 weeks compared with 6 weeks of age, a significant additional reduction in macrophage staining was found in mdx-TLR4–/– mice of the 12 week group (Fig. 5D and E).

TLR4 deficiency modifies macrophage polarization properties in mdx mice

The above findings were further validated by flow cytometry, which was performed on cellular suspensions obtained from whole diaphragms in WT, mdx and mdx-TLR4–/– mice, with infiltrating macrophages identified by positive staining for CD11b and F4/80. Absolute macrophage counts were greatly elevated in mdx diaphragms in comparison to WT, particularly during the more inflammatory phase of the disease at 6 weeks of age (Fig. 6A). The mdx-TLR4–/– mice showed a significant reduction of macrophage numbers compared with mdx at both 6 and 12 weeks (Fig. 6A and B). Therefore, these data confirm that genetic ablation of TLR4 results in lowered macrophage infiltration of dystrophic muscles during both the acute and chronic inflammatory phases of the disease.

Tissue macrophages may become activated toward a classical 'inflammatory' or an alternatively activated 'anti-inflammatory/wound healing' phenotype (24). Because resolution of inflammation is often characterized by a shift in macrophage activation characteristics toward a more anti-inflammatory phenotype, we sought to determine whether the blunting of intramuscular macrophage accumulation in mdx-TLR4–/– mice during the acute inflammatory phase of the disease was accompanied by a change in macrophage activation status. To distinguish between inflammatory and anti-inflammatory macrophage activation states, flow cytometry was employed to identify macrophages expressing iNOS and CD206 (Fig. 6C), which are considered emblematic markers for their respective ends of the macrophage polarization spectrum.

The numbers of inflammatory macrophages ($iNOS^{pos}$ $CD206^{neg}$) were greatly elevated in mdx diaphragms in comparison to WT (Fig. 6D), whereas anti-inflammatory macrophages ($iNOS^{neg}$ $CD206^{pos}$) did not differ between WT and mdx (Fig. 6E). However, the absence of TLR4 completely reversed this profile, with the $iNOS^{pos}$ $CD206^{neg}$ macrophage numbers in mdx-TLR4–/– diaphragm restored to the WT level, whereas $iNOS^{neg}$ $CD206^{pos}$ macrophages were significantly elevated compared with both mdx and WT. In addition, the median fluorescence intensity (MFI) of iNOS expression in macrophages of

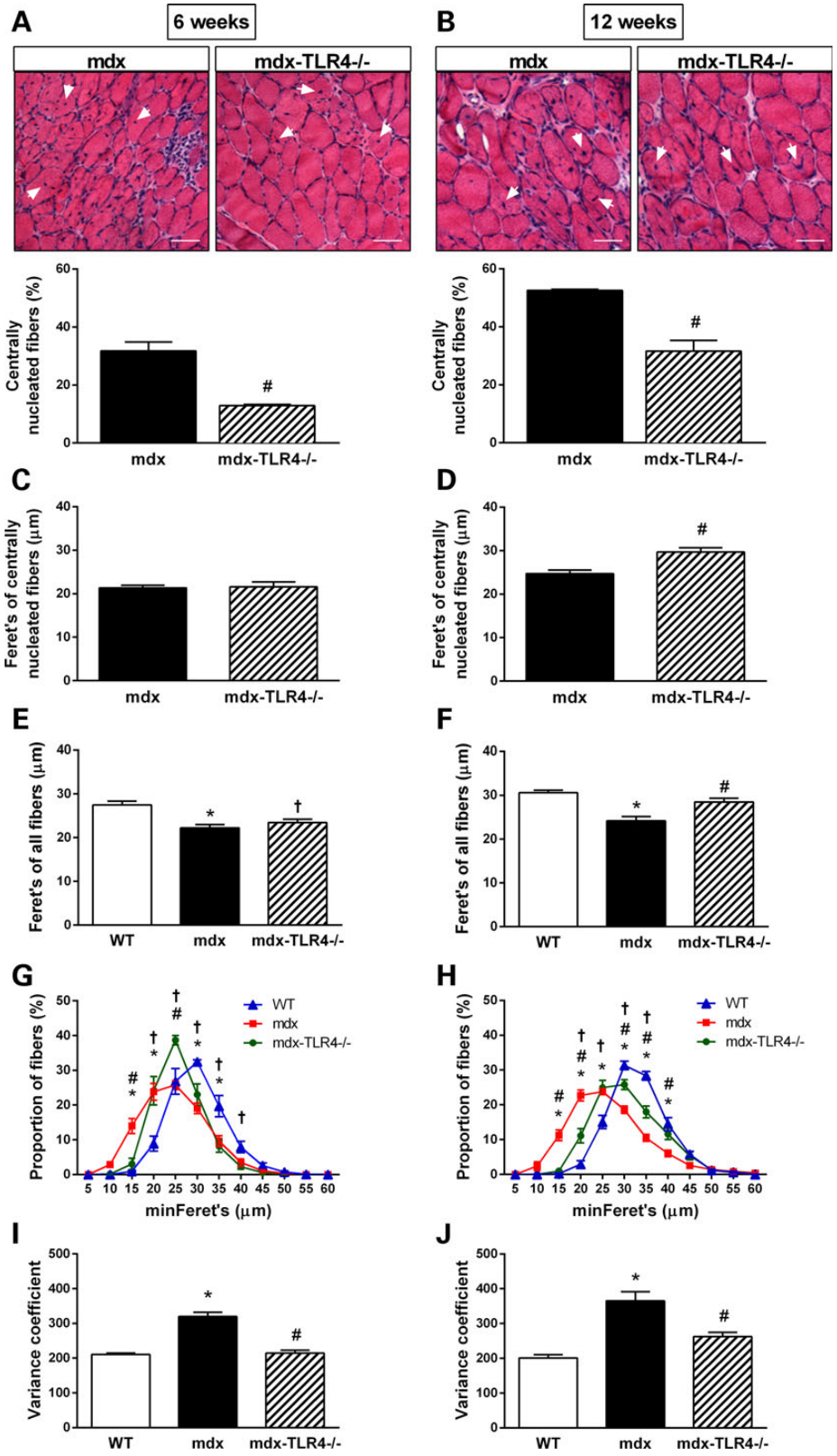

Figure 3. Muscle histopathology is reduced in mdx-TLR4–/– mice. Representative images of H&E stained diaphragm sections showing centrally nucleated fibers (white arrowheads) and their quantification in (**A**) 6-week-old and (**B**) 12-week-old mice. Minimum Feret's diameter of centrally nucleated fibers in the diaphragm at (**C**) 6 and (**D**) 12 weeks. Minimum Feret's diameter of all diaphragm fibers at (**E**) 6 and (**F**) 12 weeks. Overall fiber size distribution in diaphragms at (**G**) 6 and (**H**) 12 weeks. Mean variance coefficient of minimum Feret's diameter for all diaphragm fibers at (**I**) 6 and (**J**) 12 weeks. $N = 5–6$ mice per group; $^{\#}P < 0.01$ between mdx and mdx-TLR4–/– (by *t*-test for panels A–D), $^{*}P < 0.05$ between WT and mdx, $^{\#}P < 0.05$ between mdx and mdx-TLR4–/–, $^{\dagger}P < 0.05$ between WT and mdx-TLR4–/– (by ANOVA for panels E–J). Scale bar = 50 μm.

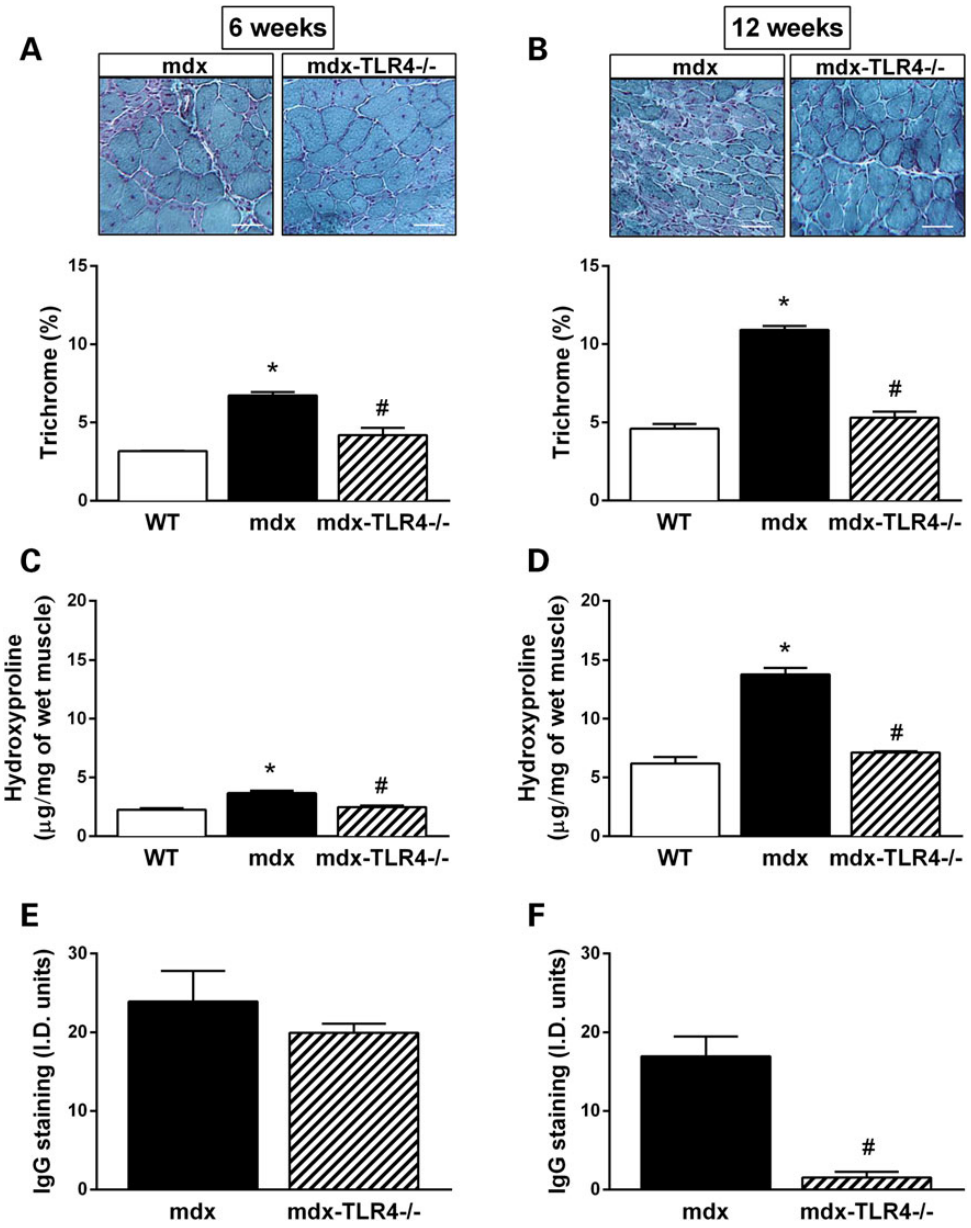

Figure 4. Collagen deposition and myofiber damage are decreased in mdx-TLR4–/– muscles. Representative images of Gomori's modified trichrome staining of diaphragm sections to quantify fibrosis at (**A**) 6 and (**B**) 12 weeks of age. Biochemical quantification of collagen deposition in diaphragms at (**C**) 6 and (**D**) 12 weeks is also shown; $N = 5$ mice per group. IgG staining to detect sarcolemmal hyperpermeability at (**E**) 6 and (**F**) 12 weeks of age; $N = 4$–6 mice per group; $^{*}P < 0.05$ between WT and mdx, $^{\#}P < 0.05$ between mdx and mdx-TLR4–/– (by ANOVA for panels A–D and by *t*-test for panels E–F). Scale bar = 50 µm, percentages of staining surface are reported to the total section area, ID = integrated density.

mdx-TLR4–/– diaphragm did not differ from WT (Fig. 6F), whereas CD206 MFI was significantly higher in mdx-TLR4–/– as compared with both WT and mdx macrophages (Fig. 6G). The tibialis anterior muscle exhibited similar reductions in macrophage infiltration and pro-inflammatory markers in the mdx-TLR4–/– group (Supplementary Material, Fig. S2 and Table S2). Therefore, the findings are collectively consistent with a shift toward greater pro-inflammatory polarization in mdx macrophages, which can be significantly prevented or reversed by a loss of TLR4 signaling.

To further investigate the macrophage polarization features associated with TLR4 deficiency, we assessed mRNA expression levels of inflammatory and anti-inflammatory polarization status-associated transcription factors (IRF5 and KLF4, respectively), as well as iNOS and CD206, in bone marrow-derived macrophages (BMDMs). The BMDMs were obtained from WT and TLR4-deficient (TLR4–/–) animals (Fig. 7, left hand panels), as well as from mdx and mdx-TLR4–/– mice (Fig. 7, right hand panels). The basal levels of iNOS, CD206 and KLF4 were all significantly elevated above WT values in the mdx group ($P < 0.05$). Upon stimulation with IFN-γ to induce pro-inflammatory polarization, there was the expected increase of iNOS (Fig. 7A) and IRF5 (Fig. 7B) in all groups. However, in comparison to the WT and mdx values, the TLR4–/– and mdx-TLR4–/– groups (respectively) exhibited relatively lower expression of these pro-inflammatory markers. In addition, after stimulation with IL-4 to promote anti-inflammatory polarization, the TLR4–/– group values of CD206 and KLF4 expression were higher than observed in

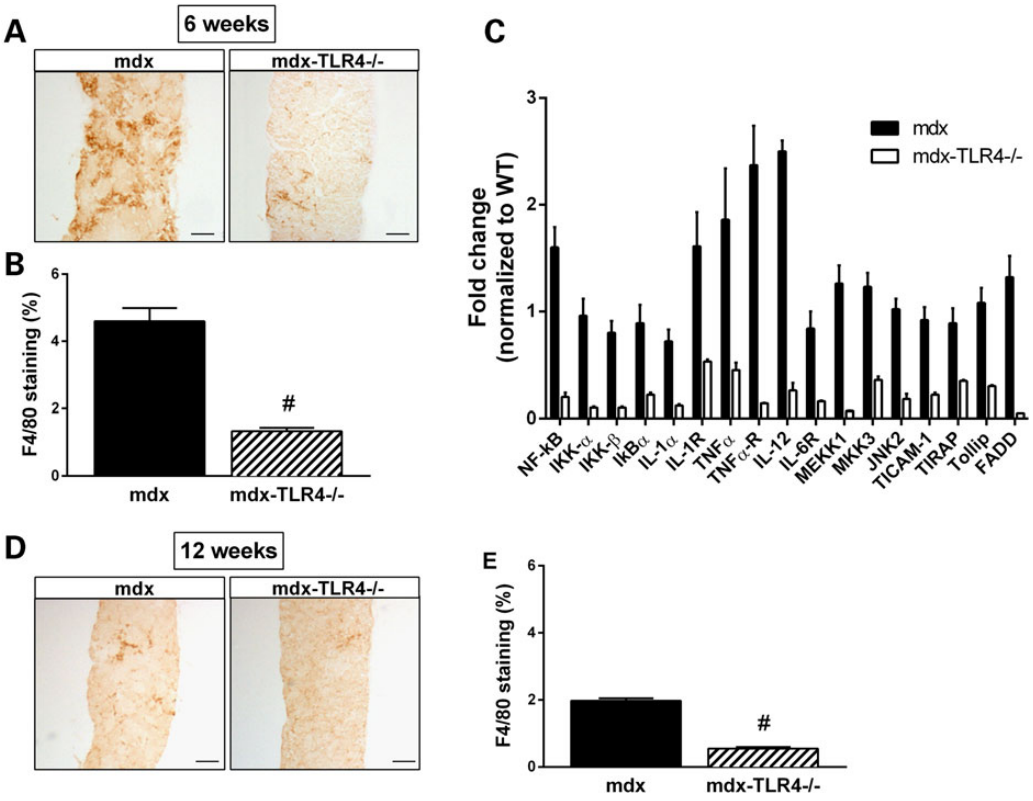

Figure 5. Genetic ablation of TLR4 reduces inflammation in the dystrophic diaphragm. (**A**) Representative images of F4/80 staining on diaphragm sections of 6-week-old mice. (**B**) Densitometric quantification of F4/80 staining in mdx and mdx-TLR4–/– diaphragms at 6 weeks of age; $N = 5$ mice per group. (**C**) Real-time PCR quantification of pro-inflammatory genes associated with Toll-like receptor signaling which were found to be significantly decreased ($P < 0.05$; $N = 9$ per group) in mdx-TLR4–/– compared with mdx diaphragms at 6 weeks of age. Data are expressed relative to age-matched WT muscles. (**D**, **E**) Images of F4/80 staining on diaphragm sections at 12 weeks and corresponding densitometric quantification. $^{\#}P < 0.01$ between mdx and mdx-TLR4–/– (by *t*-test). Scale bar = 150 μm.

WT BMDMs (Fig. 7C and D, left panel). However, a different pattern was observed in the dystrophic groups (Fig. 7C and D, right panel), in which mdx-TLR4–/– BMDMs demonstrated reduced levels of CD206 and KLF4 expression relative to mdx BMDMs under all conditions. Taken together, these *in vitro* observations suggest that the basal state of BMDMs in mdx mice is characterized by an upregulation of both pro-inflammatory and anti-inflammatory genes, whereas lack of TLR4 in this context appears to be associated with a general downregulation of gene expression at both ends of the macrophage polarization spectrum.

Glycyrrhizin treatment of mdx mice has similar beneficial effects

HMGB1, a well-established endogenous ligand of TLR4, can be released from cells passively during cellular necrosis or as an active regulated process (13). In either of the above situations, the protein must initially move out of the nucleus and into the cytoplasm. In mdx mice, immunohistochemical analysis revealed staining for HMGB1 in the cytoplasm, which was not detectable in WT muscles under the same exposure conditions (Fig. 8A–C). Interestingly, we also observed the same HMGB1 staining pattern in a small sample of human DMD muscles (Supplementary Material, Fig. 3). Furthermore, a significant increase in the total HMGB1 content of mdx muscles was confirmed by immunoblotting (Fig. 8D). Therefore, we next sought to determine whether inhibition of HMGB1 might have similar beneficial effects upon dystrophic muscle as observed in mdx mice lacking TLR4. This hypothesis was tested by treating mdx mice from 3 to 6 weeks of age with glycyrrhizin, a compound which has been shown to interfere with the biological actions of HMGB1 by binding to the two HMG-box domains of the protein (25).

In comparison to sham-treated controls, glycyrrhizin-treated mdx mice demonstrated an improved maximal force-generating capacity of the diaphragm (Fig. 8E). In addition, the proportion of centrally nucleated fibers was reduced (Fig. 8F), the size of centrally nucleated fibers (Fig. 8G) as well as all myofibers sampled (Fig. 8H) was increased, the level of fibrosis was decreased (Fig. 8I) and the amount of macrophage infiltration was blunted (Fig. 8J) in diaphragms of glycyrrhizin-treated mdx mice. Because these actions of glycyrrhizin may not be specific to the HMGB1–TLR4 interaction (26), we also treated mdx-TLR4–/– mice with glycyrrhizin in the identical manner. In general (with the exception of centrally nucleated fiber size), glycyrrhizin treatment did not confer significant additional benefits in the mdx-TLR4–/– group, suggesting that its therapeutic effects in mdx animals were primarily mediated through inhibition of the HMGB1–TLR4 axis.

Discussion

This investigation provides the first direct evidence that TLR4 acts as a key participant in the chain of events leading to chronic inflammation and progressive muscle fibrosis in muscular dystrophy caused by dystrophin deficiency. Specifically, we show that muscles of dystrophin-deficient mdx mice have increased TLR4 expression, and that genetic abrogation of TLR4 decreases

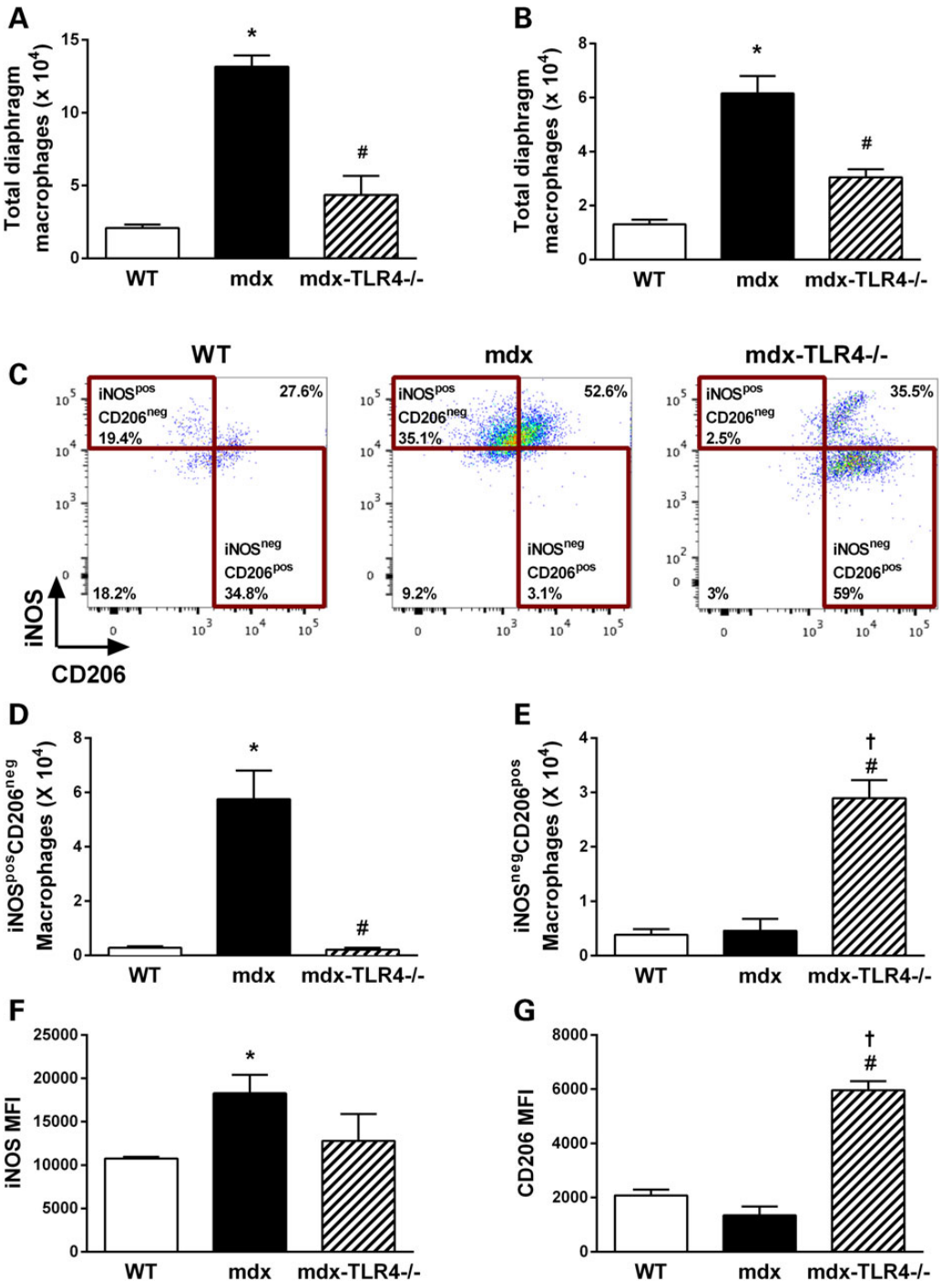

Figure 6. TLR4 ablation reduces macrophage infiltration and favors an anti-inflammatory macrophage phenotype *in vivo*. Quantification of total macrophages (CD11b + F4/80+) in WT, mdx and mdx-TLR4−/− diaphragms for (**A**) 6-week-old and (**B**) 12-week-old mice. (**C**) Representative dot plots identifying pro-inflammatory (iNOSpos CD206neg) and anti-inflammatory (iNOSneg CD206pos) macrophages in the diaphragm at 6 weeks. (**D**) Quantification of iNOSpos CD206neg macrophages. (**E**) Quantification of iNOSneg CD206pos macrophages. The median fluorescent intensities (MFI) for (**F**) iNOS and (**G**) CD206 in diaphragm-infiltrating macrophages are also shown. $N = 5–6$ mice per group; $^{*}P < 0.05$ between WT and mdx, $^{\#}P < 0.05$ between mdx and mdx-TLR4−/−, $^{\dagger}P < 0.05$ between WT and mdx-TLR4−/− (by ANOVA).

inflammation and ameliorates multiple aspects of the dystrophic disease process. In this regard, TLR4 ablation in mdx mice resulted not only in a dramatic blunting of macrophage accumulation within dystrophic muscles, but also led to an altered macrophage activation status with increased CD206 expression, which has been linked to the anti-inflammatory phenotype. This was accompanied by beneficial changes in clinically relevant endpoints including reduced fibrogenesis and improved force-generating capacity of the affected muscles. We also demonstrate that dystrophic muscles have increased levels of the TLR4 ligand HMGB1, with localization of the protein outside the nucleus as previously described in its cellular release (16). Moreover, treatment with a pharmacological inhibitor of HMGB1 (glycyrrhizin) produced similar benefits in mdx mice to those found

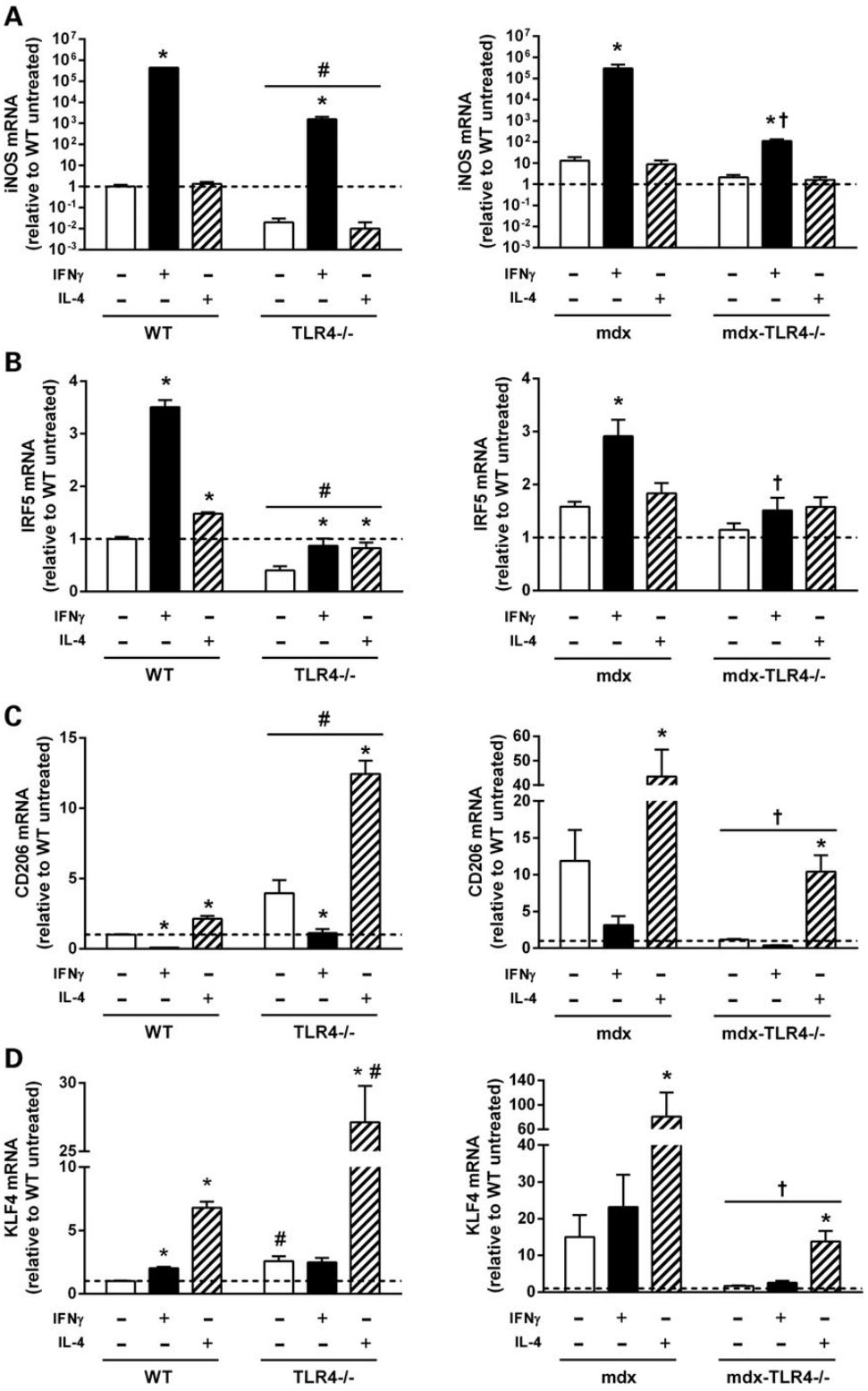

Figure 7. Genetic ablation of TLR4 influences macrophage polarization *in vitro*. Relative mRNA expression of pro-inflammatory macrophage markers (**A**) iNOS and (**B**) IRF5 as well as anti-inflammatory macrophage markers (**C**) CD206 and (**D**) KLF4 in cultured BMDMs. Cells were obtained from WT and TLR4−/− (left panels), or mdx and mdx-TLR4−/− (right panels) mice, and treated with either IFN-γ or IL-4 to favor pro-inflammatory or anti-inflammatory polarization, respectively. Values are expressed as fold-change relative to untreated WT. $N = 8–14$ per group based on two to three independent experiments; $^{*}P < 0.05$ compared with the untreated group within each mouse strain, $^{\#}P < 0.05$ between WT and TLR4−/− for a given treatment, $^{\dagger}P < 0.05$ between mdx and mdx-TLR4−/− for a given treatment (by ANOVA).

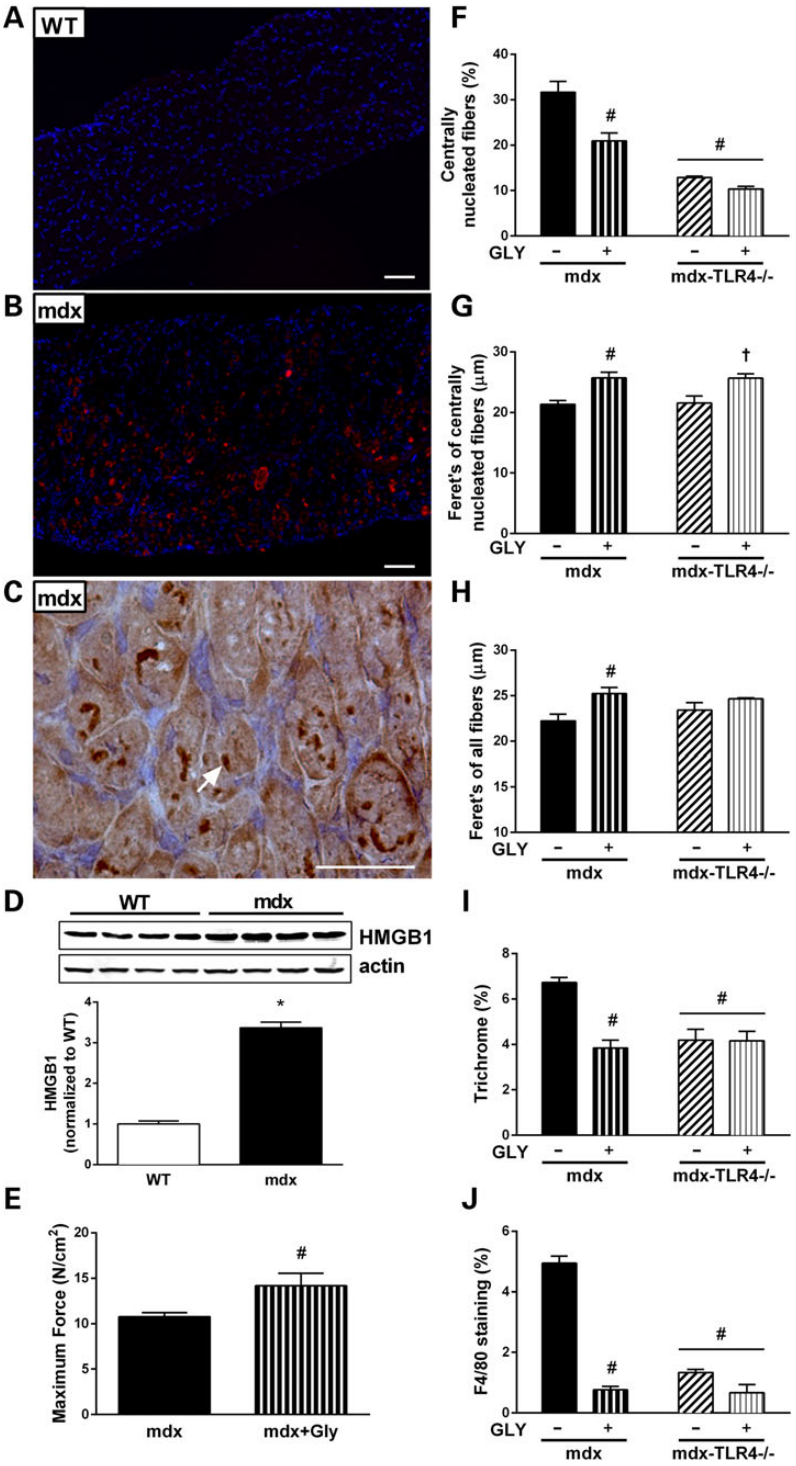

Figure 8. Glycyrrhizin treatment improves the dystrophic phenotype. HMGB1 immunofluorescence counterstained with Hoechst (blue) to identify nuclei in (**A**) WT and (**B**) mdx diaphragm transverse sections, demonstrating the presence of HMGB1 (red) outside myonuclei in the mdx group. (**C**) Higher magnification showing HMGB1 immunoreactivity (dark brown staining, as indicated by arrow) within mdx diaphragm myofibers. (**D**) Western blot quantification of HMGB1 in WT and mdx diaphragm at 6 weeks of age. (**E**) Quantification of maximum force-generating capacity of diaphragms from untreated (mdx) and glycyrrhizin-treated (mdx + Gly) mice. In diaphragms of mdx and mdx-TLR4−/− mice, either untreated (GLY-) or treated (GLY+) with glycyrrhizin, results are shown for: (**F**) proportion of centrally nucleated fibers, (**G**) minimum Feret's diameter of centrally nucleated fibers, (**H**) minimum Feret's diameter for all fibers, (**I**) quantification of Gomori's modified trichrome staining and (**J**) quantification of F4/80 staining. $N = 5$ mice per group; $^{*}P < 0.05$ compared with WT; $^{\#}P < 0.05$ comparison to untreated (GLY−) mdx and $^{\dagger}P < 0.05$ comparison between untreated (GLY−) and treated (GLY+) mdx-TLR4−/− (by *t*-test for D–E, by ANOVA for F–J). Scale bar = 50 μm.

with TLR4 ablation, but only in the presence of intact TLR4 function. Taken together, these data support the hypothesis that DAMP-mediated activation of innate immunity through TLR4 signaling plays an important role in DMD pathogenesis.

TLR4 targeting has the potential to directly affect the chemotactic properties of injured muscle fibers as well as the intrinsic properties of macrophages. With respect to the former, skeletal muscle cells express TLR4 and respond to TLR4 stimulation by greatly upregulating monocyte chemoattractant protein-1 (MCP-1/CCL2) (27), a key mediator of macrophage recruitment to injured muscles (28). In addition, low circulating levels of TLR agonists promote movement of inflammatory monocytes out of the bone marrow and into the circulation (29). This could potentially occur in DMD via TLR4 ligands released from the dystrophic muscles, such as HMGB1. Indeed, TLR4-defective mice show markedly decreased inflammation in several acute disease models including peripheral nerve injury (30), ischemia-reperfusion injury of the heart (21) or liver (31), and bleomycin (32) or cigarette smoke induced (33) lung pathology, as well as in chronic conditions such as diabetes (34), atherosclerosis and Alzheimer's disease (35). In some of these disease models the blunting of inflammation associated with TLR4 deficiency is beneficial, whereas in others it leads to less effective tissue repair. Indeed, it has been demonstrated that anti-inflammatory macrophages have the potential to either induce (36) or inhibit (37,38) fibrosis.

An important contribution of macrophages to muscle necrosis in dystrophin deficiency has been reported based on macrophage depletion experiments in young mdx mice (6). On the other hand, macrophages also play a critical role in the resolution of inflammation and tissue damage. This delicate balance is reflected by the fact that in our study, despite clear evidence for reduced tissue damage at 6 weeks of age (indicated by decreases in centrally nucleated fibers and fibrosis along with improved force), there was a persistence of fibers exhibiting abnormal sarcolemmal permeability. We speculate that this may have been due to a delay in the clearance of degenerated fibers, resulting from the lower numbers of pro-inflammatory macrophages present in the muscles of mdx-TLR4–/– mice. This would be consistent with the fact that anti-inflammatory macrophages have a relatively reduced phagocytic ability while producing various growth factors and mediators known to promote muscle regeneration (39).

The relationship between muscle histopathology parameters (e.g. inflammation, fiber degeneration and fibrosis) on the one hand, and their collective impact on maximal force-generating capacity on the other hand are complex. Although macrophage infiltration spontaneously decreased in mdx diaphragms from 6 to 12 weeks of age as expected, the amount of fibrosis in the mdx diaphragm increased several-fold during this same period. Therefore, the net effect was that diaphragm force-generating capacity remained depressed at approximately the same level over this time frame. In mdx-TLR4–/– mice, our findings suggest that the improvement of dystrophic diaphragm force generation at 6 weeks is primarily due to reduced levels of inflammatory cell infiltration and to a lesser extent decreased fibrosis, whereas at 12 weeks a larger impact of TLR4 ablation on fibrosis as well as more effective fiber regeneration (suggested by the greater size of centrally nucleated fibers) may play a greater role.

Our results are generally consistent with previous reports that modulating the macrophage polarization balance in favor of anti-inflammatory macrophages reduces the severity of dystrophic pathology in mdx mice (40,41). Interestingly, we found that BMDMs lacking TLR4 from both non-dystrophic and dystrophic mice exhibited a relative hyporesponsiveness to stimulation by IFN-γ, suggesting resistance to pro-inflammatory polarization. However, the situation was more complex in BMDMs from mdx mice, which demonstrated basal upregulation of both pro-inflammatory and anti-inflammatory marker genes. Intriguingly, despite the anti-inflammatory skewing found in mdx-TLR4–/– intramuscular macrophages *in vivo*, BMDMs from mdx-TLR4–/– mice appeared to be hyporesponsive to both pro-inflammatory and anti-inflammatory polarization stimuli *in vitro*. This would appear to indicate that these TLR4-deficient macrophages required additional cues *in vivo* to promote anti-inflammatory polarization in dystrophic muscles. It also suggests that TLR4-deficient macrophages could be defective in other functions, such as in the instruction of adaptive immunity, and we do not rule out the possibility of additional effects upon lymphocytes and other inflammatory cell types implicated in DMD pathology (5,42).

The DAMPs which are reportedly able to activate TLR4 under pathological conditions include extracellular matrix components [e.g. hyaluronic acid (32,43), fibronectin extradomain A (44), biglycan (45), fibrinogen (46,47), heat shock proteins (e.g. HSP70) and molecules normally found in the nucleus (e.g. HMGB1), as well as others (11,12). HMGB1 is a non-histone nuclear protein, which can be either passively released (from dying cells) or actively secreted (principally demonstrated in monocytes/macrophages) into the extracellular milieu in response to tissue injury (13). In the case of active secretion, there is involvement of a non-classical secretory pathway in which HMGB1 is sequestered within cytoplasmic vesicles prior to being exported (16). In our study, punctate staining for HMGB1 was identified in the cytoplasm of non-necrotic fibers from both humans and mice with muscular dystrophy, suggesting the possibility of active secretion. Similar staining for HMGB1 has also been reported in non-necrotic muscle fibers of patients with idiopathic inflammatory myopathies (48). An additional potential source of HMGB1 is the large number of infiltrating macrophages within dystrophic muscles. Although HMGB1 is but one of several potential DAMPs capable of activating TLR4, it has a number of features which make it a particularly good candidate for playing a role in muscular dystrophy. First, HMGB1 binding to TLR4 has been implicated in macrophage activation and recruitment (49). Second, HMGB1 has the capacity to trigger NF-kB activation and associated cytokine/chemokine production (50), which are also implicated in the progression of Duchenne dystrophy. Third, there is evidence that HMGB1 can directly contribute to contractile dysfunction in skeletal muscle by impairing calcium release from the sarcoplasmic reticulum (48).

The agent used to inhibit HMGB1 in this study, glycyrrhizin, is a glycoconjugated triterpene produced by the licorice plant *Glycyrrhiza glabra* (25). Glycyrrhizin inhibits HMGB1 by binding both of its HMG boxes, thereby preventing its cytokine-inducing and mononuclear cell recruitment actions (25,51,52). It should be noted that glycyrrhizin may also have had effects on other pathways such as phospholipase A2 (26), and HMGB1 has several putative cell surface receptors besides TLR4, including TLR2 and RAGE (53). However, the fact that glycyrrhizin treatment had little or no impact upon fibrosis, fiber size, inflammation and proportion of centrally nucleated fibers in mdx-TLR4–/– mice suggests (but does not prove) that inhibition of the HMGB1–TLR4 axis is likely to have been its primary mechanism of action in mitigating mdx muscle pathology.

Although not previously recognized as such, indirect evidence from prior investigations also supports a role for TLR4 signaling in muscular dystrophy pathogenesis. For instance, mdx

mice which are deficient in another putative TLR4 ligand, fibrinogen (46,47), show reduced macrophage infiltration and decreased fibrosis in the diaphragm (54). In addition, overexpression of A20, a negative regulator of TLR-MyD88 signaling, has beneficial effects upon muscle inflammation in mdx mice (55). Interestingly, intramuscular injection of recombinant human biglycan protein has been reported to mitigate muscle pathology in mdx mice (56). However, the form of biglycan used in that study may have lacked the glycosaminoglycans side chains required for TLR activation, potentially producing an antagonistic effect upon TLR4 signaling. It is notable that other TLR members such as TLR7/8/9 and their endogenous ligands, the single-stranded ribonucleic acids (ssRNAs), have also been highlighted as important contributors to disease progression in dystrophin-deficient and dysferlin-deficient muscles (57,58).

In summary, this study adds to a steadily enlarging literature which points to interactions between TLR4 and tissue-derived DAMPs as being important in the initiation as well as the maintenance of sterile inflammation (12). While partial inhibition of TLR4 could in principle be an effective therapeutic measure in DMD, given the theoretical risk of increased infectious complications with this approach, it may be more attractive from a clinical standpoint to target endogenous TLR4 ligands such as HMGB1. It is noteworthy that glycyrrhizin can be administered orally to humans and has been used to treat patients with hepatitis (25,59,60). The potential of glycyrrhizin and other pharmacological agents to prevent the adverse consequences of DAMP-mediated TLR4 signaling deserves further investigation in DMD. In addition, the effectiveness of such immune modulation treatment in DMD will likely depend greatly upon the specific stage of disease at which it is introduced, and efforts to determine the most appropriate therapeutic window, perhaps guided by non-invasive biomarkers to assess DAMP-mediated activation of the innate immune system, should be pursued in future studies.

Materials and Methods

Animals

Wild-type (WT; C57BL/10) and mdx (C57BL/10ScSn-Dmd^{mdx}/J) mouse breeding pairs were originally purchased from The Jackson Laboratories (Bar Harbor, ME); mice lacking TLR4 (TLR4–/–) were kindly provided by S. Akira (Osaka University, Japan). TLR4–/– mice were on the C57BL/6 background, and males were crossed with homozygous mdx females to produce male mdx mice that were heterozygous for the TLR4 mutation. These animals were then bred with homozygous mdx females to generate mdx mice of both sexes heterozygous for the TLR4 mutation. The latter were bred together to create the mdx-TLR4–/– mice homozygous for the TLR4 mutation, which were thus on a majority (75%) C57BL/10 and minority (25%) C57BL/6 background. The mdx controls and WT mice were on the C57BL/10 background. It should be noted that a previous study (61) reported no differences in inflammation, fibrosis or myofiber damage between mdx mice on the BL/6 and BL/10 background strains. Mice were screened for the TLR4 mutation by PCR. The animals were euthanized at either 6 or 12 weeks of age, at which time both the diaphragm and tibialis anterior muscles were removed. Mice were maintained in a controlled pathogen-free facility throughout the course of study. All animal procedures were approved by the McGill University Animal Care and Use Committee, in accordance with the guidelines issued by the Canadian Council on Animal Care.

Histological analysis

Excised muscles were quickly frozen in liquid nitrogen-cooled 2-methylbutane (Fisher, Fairlawn, NJ) and stored at –80°C. For general morphology, cryostat sections were stained with hematoxylin and eosin (H&E) according to standard protocols. Bright-field images were photographed using an Olympus BX51 microscope with a QImaging Retiga 2000R camera system. A grid with a fixed square width was randomly applied onto each section to quantify (i) the proportion of fibers with central myonuclei and (ii) the minimum Feret's diameter of myofibers (62). As an index of muscle pathology, we also determined the variance coefficient of muscle fiber size using the formula: variance coefficient = (standard deviation of the muscle fiber size/mean muscle fiber size) × 1000 as previously described (62). The measurements were taken on myofibers inside five squares randomly chosen using ImageJ software (63). For each tissue section analyzed, a minimum of 500 muscle fibers were counted. To evaluate the level of muscle infiltration by macrophages, tissue sections were immunostained with anti-F4/80 (Abcam ab6640) and the percentage of positively stained area on the entire muscle section area was quantified using a red green blue (RGB) Threshold color plugin of ImageJ. Briefly, the range of RGB colors involved in the positive staining is selected and the pixel surface of the selection calculated. The surface value of the staining is then expressed as a percentage of the total tissue section surface. Muscle fibrosis was assessed by staining transverse muscle sections using Gomori's modified trichrome method (3) and quantified in a similar manner. IgG staining was performed on frozen muscle sections to assess myofiber sarcolemmal permeability as previously described (64) using an anti-mouse IgG HRP-conjugated antibody (Promega, W402B); the integrated density of IgG staining (product of the positively stained area and the mean gray value) was quantified using ImageJ and reported to the entire muscle section area. For HMGB1 staining, human and mouse tissue sections were fixed in cold acetone at –20°C, permeabilized in phosphate buffered saline (PBS)/0.1% Triton X-100 for 20 min, washed three times in PBS, blocked in 3% bovine serum albumin (BSA) for 1 h at room temperature and incubated overnight at 4°C with anti-HMGB1 (Abcam ab18256). Sections were then washed three times with PBS and incubated with a Cy3 secondary antibody (Jackson ImmunoResearch 111-165-144) for 1 h at room temperature, washed three times with PBS/0.04% saponin and counterstained with Hoechst 33342 (Sigma). For HMGB1 immunoperoxidase staining, a biotinylated secondary antibody (Jackson Immunosearch 111-065-003) was used followed by counterstaining with hematoxylin for 1 min.

Hydroxyproline assay

Collagen content of muscle was determined by quantifying hydroxyproline content in muscle as described previously (3). The muscles were homogenized in 0.5 mol/l glacial acetic acid, dried in a speed vacuum and weighed. The dried samples were hydrolyzed in 6 N HCl at 110°C overnight. Following acid hydrolysis, 10 μl (diaphragm) or 20 μl (tibialis anterior) samples were dried and resuspended in citrate-acetate buffer. Freshly prepared chloramine-T solution was added to the dried samples and allowed to stand at room temperature for 20 min. Freshly prepared Ehrlich's solution was next added and the samples were heated to 65°C for 15 min. The processed samples were transferred to a 96-well plate and optical densities were read at 550 nm. For each assay, a standard curve was generated using known concentrations of hydroxyproline, and the sample hydroxyproline content (per mg of wet

muscle) was estimated by comparing their ODs to the standard curve. All chemicals were purchased from Sigma.

Western blotting

Protein lysates from cell culture or muscles were centrifuged at 15,000 × *g* in 4°C for 20 min and the resulting supernatants were assayed for protein quantity by the Bradford method. The dilutions of primary antibodies (IkBα: Cell Signaling 4814; p-IkBα: Cell Signaling 2859; HMGB1: Abcam ab18256; actin: Sigma A3853) and secondary antibodies (IkBα: Promega W402B; p-IkBα: Promega W401B; HMGB1: Li-Cor 926-32211; actin: Thermo Scientific 35518) were made as per the manufacturers' instructions. Both IkBα and p-IkBα were incubated with SuperSignal® West Femto substrate (Thermo Scientific 34095). The quantification of specific protein bands was performed using the Odyssey® Infrared Imaging System (LI-COR® Biosciences, Lincoln, NE) for HMGB1 and with ChemiDoc™ Image Lab™ 5.0 (Bio-Rad) for IkBα. Ponceau S (Sigma P7170) or actin was used as protein loading control.

Real-time PCR quantification of gene expression

Total RNA was extracted from tissues or cells using TRIzol reagent (Invitrogen, USA) according to the manufacturer's protocol. RNA was treated with DNase I (Gibco, USA), purified using the RNeasy minikit (Qiagen, Germany), and then quantified by spectrophotometric optical density measurement. The purified RNA was reverse transcribed to cDNA with random primers and SuperScript II (Invitrogen, USA) reverse transcriptase. Quantitative RT-PCR was performed using 5 ng of cDNA mixed with 10 µl SYBR® Green Master Mixes (SABiosciences, USA) and 1 µl of 10 µM primer mixes. RT-PCR was carried out for 40 cycles at a melting temperature of 95°C for 15 s and an annealing temperature of 60°C for 1 min using a StepOne Plus Thermocycler (Applied Biosystems, USA). Mouse HPRT1 was used as an internal control. The relative quantification of gene expression was analyzed by the $2^{-\Delta\Delta Ct}$ method, and the results are expressed as *n*-fold difference relative to the corresponding WT strain. TLR signaling pathways were analyzed using a commercial RT-PCR array (RT^2 Profiler™ PCR Array System, SABiosciences); other primer sequences are shown in Supplementary Material, Table S3.

Evaluation of force-generating capacity

As previously described in detail (65), the diaphragm was removed and placed into equilibrated (95% O_2–5% CO_2; pH 7.38) Krebs solution. After attaching the diaphragm strip to a force transducer/length servomotor system (model 300B; dual mode; Cambridge Technology, Watertown, MA), optimal length (*Lo*) was determined. The force–frequency relationship was measured by sequential supramaximal stimulation for 1 s at 10, 30, 50, 100 and 150 Hz, with 2 min between each stimulation train. Muscle force was normalized to cross-sectional area and expressed as Newtons/cm^2.

Flow cytometry

Skeletal muscle macrophages were characterized and quantified in WT, mdx and mdx-TLR4–/– animals at 6 and 12 weeks of age. Single cell suspensions were obtained by mincing the muscles into small pieces in ice-cold PBS. The muscle pieces were incubated in buffered 0.2% collagenase B (Roche) solution for 1 h at 37°C followed by filtering of the cell suspension through a 70-µm cell strainer. Total viable cell numbers were determined by Trypan blue stain exclusion and were used to calculate absolute cell counts. Following red cell lysis, the cells were resuspended in FACS buffer (PBS with 0.5% BSA) and pre-incubated in blocking solution (anti-CD16/CD32, BD Biosciences). The cells were then stained using the following fluorescently labeled antibodies for 20 min at 4°C: VF00 labeled anti-mouse CD45 (BD Biosciences); Alexa Fluor 488 labeled anti-mouse CD11b and PE-Cy7 labeled anti-mouse F4/80 (all from BioLegend). Alternatively, after similar lysing and blocking steps, cells were stained for VF00 labeled anti-mouse CD45 (BD Biosciences), APC-Cy7 labeled anti-mouse CD11b, PE-Cy7 labeled anti-mouse F4/80 and APC labeled anti-mouse CD206 (all from BioLegend). Following staining with surface markers, cells were washed, fixed in 4% paraformaldehyde and permeabilized using PBS/0.3% Triton. The cells were then stained intracellularly with fluorescein isothiocyanate labeled anti-mouse iNOS (BD Biosciences). Stained cells were washed to remove excess antibodies, resuspended in FACS buffer and acquired on a BD LSR-II. For each sample, 100 000–500 000 events were recorded. Data analysis was done using FlowJo software (Treestar Inc., Ashland, OR, USA). CD45+ cells were first gated, followed by identification of CD11b + F4/80+ events; iNOS and CD206 expression were also assessed on the populations thus generated. Appropriate isotype controls were used to set negative population gates. Absolute numbers of macrophages were calculated by multiplying percentages determined from flow cytometry by the quantity of cells isolated per muscle.

Bone marrow-derived macrophage cultures

To isolate bone marrow cells, femur and tibiae were cut open at the epiphyses and the marrow flushed out using Roswell Park Memorial Institute (RPMI) medium. The cells were washed with RPMI and counted using Trypan Blue staining. Cells were plated onto 6-well plates at a frequency of 5×10^6 cells/well and cultured for 7 days in complete RPMI supplemented with 10% fetal bovine serum (FBS) and 10% L929 conditioned medium (containing macrophage-colony stimulating factor). The adherent cells at the end of 7 day culture were treated with either pro-inflammatory stimulus IFN-γ (20 ng/ml) or anti-inflammatory stimulus IL-4 (20 ng/ml) for 24 h (66). Untreated naive macrophages from WT were used as controls.

Glycyrrhizin treatment

Three-week-old mdx or mdx-TLR4–/– mice were given drinking water containing 0.05% (wt/vol) of glycyrrhizin (Sigma) for 3 weeks. The solution was prepared fresh three times per week after 5 h of stirring at 37°C to dissolve glycyrrhizin at this concentration as previously described (67). This dose was well tolerated by the animals with no apparent signs of toxicity.

Statistical analysis

All data are expressed as group mean values ± SE. Data were analyzed using a commercial software package (GraphPad Prism, San Diego, CA, USA). Significant differences between groups were determined by t-test (if two groups), or by ANOVA with post-hoc application of the Tukey test to adjust for multiple comparisons (if more than two groups). Statistical significance was set at $P < 0.05$.

Supplementary Material

Supplementary Material is available at *HMG* online.

Acknowledgements

We are grateful for excellent technical help from Fazila Chouiali for immunofluorescence image acquisition. We thank Dr Audrey Poon for critical reading of the manuscript.

Conflict of Interest statement. The authors declare they have no conflicts of interest.

Funding

This study was financially supported by Canadian Institutes of Health Research, Fonds de la Recherche en Santé du Quebec and McGill University Health Centre Research Institute.

References

1. Petrof, B.J. (2002) Molecular pathophysiology of myofiber injury in deficiencies of the dystrophin-glycoprotein complex. *Am. J. Phys. Med. Rehabil.*, **81**, S162–S174.
2. Manzur, A.Y., Kuntzer, T., Pike, M. and Swan, A. (2008) Glucocorticoid corticosteroids for Duchenne muscular dystrophy. *Cochrane. Database. Syst. Rev.*, doi: 10.1002/14651858.CD003725.pub3.
3. Stedman, H.H., Sweeney, H.L., Shrager, J.B., Maguire, H.C., Panettieri, R.A., Petrof, B., Narusawa, M., Leferovich, J.M., Sladky, J.T. and Kelly, A.M. (1991) The mdx mouse diaphragm reproduces the degenerative changes of Duchenne muscular dystrophy. *Nature*, **352**, 536–539.
4. Morrison, J., Lu, Q.L., Pastoret, C., Partridge, T. and Bou-Gharios, G. (2000) T-cell-dependent fibrosis in the mdx dystrophic mouse. *Lab Invest.*, **80**, 881–891.
5. Wehling-Henricks, M., Sokolow, S., Lee, J.J., Myung, K.H., Villalta, S.A. and Tidball, J.G. (2008) Major basic protein-1 promotes fibrosis of dystrophic muscle and attenuates the cellular immune response in muscular dystrophy. *Hum. Mol. Genet.*, **17**, 2280–2292.
6. Wehling, M., Spencer, M.J. and Tidball, J.G. (2001) A nitric oxide synthase transgene ameliorates muscular dystrophy in mdx mice. *J. Cell Biol.*, **155**, 123–131.
7. Acharyya, S., Villalta, S.A., Bakkar, N., Bupha-Intr, T., Janssen, P.M., Carathers, M., Li, Z.W., Beg, A.A., Ghosh, S., Sahenk, Z. *et al.* (2007) Interplay of IKK/NF-kappaB signaling in macrophages and myofibers promotes muscle degeneration in Duchenne muscular dystrophy. *J. Clin. Invest.*, **117**, 889–901.
8. Radley, H.G., Davies, M.J. and Grounds, M.D. (2008) Reduced muscle necrosis and long-term benefits in dystrophic mdx mice after cV1q (blockade of TNF) treatment. *Neuromuscul. Disord.*, **18**, 227–238.
9. Chen, Y.W., Nagaraju, K., Bakay, M., McIntyre, O., Rawat, R., Shi, R. and Hoffman, E.P. (2005) Early onset of inflammation and later involvement of TGFbeta in Duchenne muscular dystrophy. *Neurology*, **65**, 826–834.
10. Kawai, T. and Akira, S. (2010) The role of pattern-recognition receptors in innate immunity: update on Toll-like receptors. *Nat. Immunol.*, **11**, 373–384.
11. Bianchi, M.E. (2007) DAMPs, PAMPs and alarmins: all we need to know about danger. *J. Leukoc. Biol.*, **81**, 1–5.
12. Chen, G.Y. and Nunez, G. (2010) Sterile inflammation: sensing and reacting to damage. *Nat. Rev. Immunol.*, **10**, 826–837.
13. Klune, J.R., Dhupar, R., Cardinal, J., Billiar, T.R. and Tsung, A. (2008) HMGB1: endogenous danger signaling. *Mol. Med.*, **14**, 476–484.
14. Scaffidi, P., Misteli, T. and Bianchi, M.E. (2002) Release of chromatin protein HMGB1 by necrotic cells triggers inflammation. *Nature*, **418**, 191–195.
15. Xu, H., Su, Z., Wu, J., Yang, M., Penninger, J.M., Martin, C.M., Kvietys, P.R. and Rui, T. (2010) The alarmin cytokine, high mobility group box 1, is produced by viable cardiomyocytes and mediates the lipopolysaccharide-induced myocardial dysfunction via a TLR4/phosphatidylinositol 3-kinase gamma pathway. *J. Immunol.*, **184**, 1492–1498.
16. Gardella, S., Andrei, C., Ferrera, D., Lotti, L.V., Torrisi, M.R., Bianchi, M.E. and Rubartelli, A. (2002) The nuclear protein HMGB1 is secreted by monocytes via a non-classical, vesicle-mediated secretory pathway. *EMBO Rep.*, **3**, 995–1001.
17. Wang, H., Bloom, O., Zhang, M., Vishnubhakat, J.M., Ombrellino, M., Che, J., Frazier, A., Yang, H., Ivanova, S., Borovikova, L. *et al.* (1999) HMG-1 as a late mediator of endotoxin lethality in mice. *Science*, **285**, 248–251.
18. Andrassy, M., Volz, H.C., Igwe, J.C., Funke, B., Eichberger, S.N., Kaya, Z., Buss, S., Autschbach, F., Pleger, S.T., Lukic, I.K. *et al.* (2008) High-mobility group box-1 in ischemia-reperfusion injury of the heart. *Circulation*, **117**, 3216–3226.
19. Caso, J.R., Pradillo, J.M., Hurtado, O., Lorenzo, P., Moro, M.A. and Lizasoain, I. (2007) Toll-like receptor 4 is involved in brain damage and inflammation after experimental stroke. *Circulation*, **115**, 1599–1608.
20. Okuma, Y., Liu, K., Wake, H., Zhang, J., Maruo, T., Date, I., Yoshino, T., Ohtsuka, A., Otani, N., Tomura, S. *et al.* (2012) Anti-high mobility group box-1 antibody therapy for traumatic brain injury. *Ann. Neurol.*, **72**, 373–384.
21. Oyama, J., Blais, C. Jr, Liu, X., Pu, M., Kobzik, L., Kelly, R.A. and Bourcier, T. (2004) Reduced myocardial ischemia-reperfusion injury in Toll-like receptor 4-deficient mice. *Circulation*, **109**, 784–789.
22. Karpati, G., Carpenter, S. and Prescott, S. (1988) Small-caliber skeletal muscle fibers do not suffer necrosis in mdx mouse dystrophy. *Muscle Nerve*, **11**, 795–803.
23. Villalta, S.A., Nguyen, H.X., Deng, B., Gotoh, T. and Tidball, J.G. (2009) Shifts in macrophage phenotypes and macrophage competition for arginine metabolism affect the severity of muscle pathology in muscular dystrophy. *Hum. Mol. Genet.*, **18**, 482–496.
24. Sica, A. and Mantovani, A. (2012) Macrophage plasticity and polarization: in vivo veritas. *J. Clin. Invest.*, **122**, 787–795.
25. Mollica, L., De Marchis, F., Spitaleri, A., Dallacosta, C., Pennacchini, D., Zamai, M., Agresti, A., Trisciuoglio, L., Musco, G. and Bianchi, M.E. (2007) Glycyrrhizin binds to high-mobility group box 1 protein and inhibits its cytokine activities. *Chem. Biol.*, **14**, 431–441.
26. Okimasu, E., Moromizato, Y., Watanabe, S., Sasaki, J., Shiraishi, N., Morimoto, Y.M., Miyahara, M. and Utsumi, K. (1983) Inhibition of phospholipase A2 and platelet aggregation by glycyrrhizin, an antiinflammation drug. *Acta Med. Okayama*, **37**, 385–391.
27. Boyd, J.H., Divangahi, M., Yahiaoui, L., Gvozdic, D., Qureshi, S. and Petrof, B.J. (2006) Toll-like receptors differentially regulate CC and CXC chemokines in skeletal muscle via NF-kappaB and calcineurin. *Infect. Immun.*, **74**, 6829–6838.
28. Lu, H., Huang, D., Ransohoff, R.M. and Zhou, L. (2011) Acute skeletal muscle injury: CCL2 expression by both monocytes and injured muscle is required for repair. *FASEB J.*, **25**, 3344–3355.
29. Shi, C., Jia, T., Mendez-Ferrer, S., Hohl, T.M., Serbina, N.V., Lipuma, L., Leiner, I., Li, M.O., Frenette, P.S. and Pamer, E.G. (2011) Bone marrow mesenchymal stem and progenitor

cells induce monocyte emigration in response to circulating Toll-like receptor ligands. *Immunity*, **34**, 590–601.
30. Boivin, A., Pineau, I., Barrette, B., Filali, M., Vallieres, N., Rivest, S. and Lacroix, S. (2007) Toll-like receptor signaling is critical for Wallerian degeneration and functional recovery after peripheral nerve injury. *J. Neurosci.*, **27**, 12565–12576.
31. Tsung, A., Klune, J.R., Zhang, X., Jeyabalan, G., Cao, Z., Peng, X., Stolz, D.B., Geller, D.A., Rosengart, M.R. and Billiar, T.R. (2007) HMGB1 release induced by liver ischemia involves Toll-like receptor 4 dependent reactive oxygen species production and calcium-mediated signaling. *J. Exp. Med.*, **204**, 2913–2923.
32. Jiang, D., Liang, J., Fan, J., Yu, S., Chen, S., Luo, Y., Prestwich, G. D., Mascarenhas, M.M., Garg, H.G., Quinn, D.A. *et al.* (2005) Regulation of lung injury and repair by Toll-like receptors and hyaluronan. *Nat. Med.*, **11**, 1173–1179.
33. Doz, E., Noulin, N., Boichot, E., Guenon, I., Fick, L., Le, B.M., Lagente, V., Ryffel, B., Schnyder, B., Quesniaux, V.F. *et al.* (2008) Cigarette smoke-induced pulmonary inflammation is TLR4/MyD88 and IL-1R1/MyD88 signaling dependent. *J. Immunol.*, **180**, 1169–1178.
34. Shi, H., Kokoeva, M.V., Inouye, K., Tzameli, I., Yin, H. and Flier, J.S. (2006) TLR4 links innate immunity and fatty acid-induced insulin resistance. *J. Clin. Invest.*, **116**, 3015–3025.
35. Stewart, C.R., Stuart, L.M., Wilkinson, K., van Gils, J.M., Deng, J., Halle, A., Rayner, K.J., Boyer, L., Zhong, R., Frazier, W.A. *et al.* (2010) CD36 ligands promote sterile inflammation through assembly of a Toll-like receptor 4 and 6 heterodimer. *Nat. Immunol.*, **11**, 155–161.
36. Serrano, A.L. and Munoz-Canoves, P. (2010) Regulation and dysregulation of fibrosis in skeletal muscle. *Exp. Cell Res.*, **316**, 3050–3058.
37. Pesce, J.T., Ramalingam, T.R., Mentink-Kane, M.M., Wilson, M. S., El Kasmi, K.C., Smith, A.M., Thompson, R.W., Cheever, A. W., Murray, P.J. and Wynn, T.A. (2009) Arginase-1-expressing macrophages suppress Th2 cytokine-driven inflammation and fibrosis. *PLoS. Pathog.*, **5**, e1000371.
38. Wilson, M.S., Elnekave, E., Mentink-Kane, M.M., Hodges, M.G., Pesce, J.T., Ramalingam, T.R., Thompson, R.W., Kamanaka, M., Flavell, R.A., Keane-Myers, A. *et al.* (2007) IL-13Ralpha2 and IL-10 coordinately suppress airway inflammation, airway-hyperreactivity, and fibrosis in mice. *J. Clin. Invest.*, **117**, 2941–2951.
39. Tidball, J.G. and Villalta, S.A. (2010) Regulatory interactions between muscle and the immune system during muscle regeneration. *Am. J. Physiol. Regul. Integr. Comp. Physiol.*, **298**, R1173–R1187.
40. Villalta, S.A., Deng, B., Rinaldi, C., Wehling-Henricks, M. and Tidball, J.G. (2011) IFN-gamma promotes muscle damage in the mdx mouse model of Duchenne muscular dystrophy by suppressing M2 macrophage activation and inhibiting muscle cell proliferation. *J. Immunol.*, **187**, 5419–5428.
41. Villalta, S.A., Rinaldi, C., Deng, B., Liu, G., Fedor, B. and Tidball, J.G. (2011) Interleukin-10 reduces the pathology of mdx muscular dystrophy by deactivating M1 macrophages and modulating macrophage phenotype. *Hum. Mol. Genet.*, **20**, 790–805.
42. Vetrone, S.A., Montecino-Rodriguez, E., Kudryashova, E., Kramerova, I., Hoffman, E.P., Liu, S.D., Miceli, M.C. and Spencer, M.J. (2009) Osteopontin promotes fibrosis in dystrophic mouse muscle by modulating immune cell subsets and intramuscular TGF-beta. *J. Clin. Invest*, **119**, 1583–1594.
43. Taylor, K.R., Yamasaki, K., Radek, K.A., Di, N.A., Goodarzi, H., Golenbock, D., Beutler, B. and Gallo, R.L. (2007) Recognition of hyaluronan released in sterile injury involves a unique receptor complex dependent on Toll-like receptor 4, CD44, and MD-2. *J. Biol. Chem.*, **282**, 18265–18275.
44. Okamura, Y., Watari, M., Jerud, E.S., Young, D.W., Ishizaka, S. T., Rose, J., Chow, J.C. and Strauss, J.F. III (2001) The extra domain A of fibronectin activates Toll-like receptor 4. *J. Biol. Chem.*, **276**, 10229–10233.
45. Schaefer, L., Babelova, A., Kiss, E., Hausser, H.J., Baliova, M., Krzyzankova, M., Marsche, G., Young, M.F., Mihalik, D., Gotte, M. *et al.* (2005) The matrix component biglycan is proinflammatory and signals through Toll-like receptors 4 and 2 in macrophages. *J. Clin. Invest*, **115**, 2223–2233.
46. Smiley, S.T., King, J.A. and Hancock, W.W. (2001) Fibrinogen stimulates macrophage chemokine secretion through Toll-like receptor 4. *J. Immunol.*, **167**, 2887–2894.
47. Barrera, V., Skorokhod, O.A., Baci, D., Gremo, G., Arese, P. and Schwarzer, E. (2011) Host fibrinogen stably bound to hemozoin rapidly activates monocytes via TLR-4 and CD11b/CD18-integrin: a new paradigm of hemozoin action. *Blood*, **117**, 5674–5682.
48. Grundtman, C., Bruton, J., Yamada, T., Ostberg, T., Pisetsky, D. S., Harris, H.E., Andersson, U., Lundberg, I.E. and Westerblad, H. (2010) Effects of HMGB1 on in vitro responses of isolated muscle fibers and functional aspects in skeletal muscles of idiopathic inflammatory myopathies. *FASEB J.*, **24**, 570–578.
49. Yang, H., Hreggvidsdottir, H.S., Palmblad, K., Wang, H., Ochani, M., Li, J., Lu, B., Chavan, S., Rosas-Ballina, M., Al-Abed, Y. *et al.* (2010) A critical cysteine is required for HMGB1 binding to Toll-like receptor 4 and activation of macrophage cytokine release. *Proc. Natl. Acad. Sci. USA*, **107**, 11942–11947.
50. Lv, B., Wang, H., Tang, Y., Fan, Z., Xiao, X. and Chen, F. (2009) High-mobility group box 1 protein induces tissue factor expression in vascular endothelial cells via activation of NF-kappaB and Egr-1. *Thromb. Haemost.*, **102**, 352–359.
51. Mabuchi, A., Wake, K., Marlini, M., Watanabe, H. and Wheatley, A.M. (2009) Protection by glycyrrhizin against warm ischemia-reperfusion-induced cellular injury and derangement of the microcirculatory blood flow in the rat liver. *Microcirculation*, **16**, 364–376.
52. Schiraldi, M., Raucci, A., Munoz, L.M., Livoti, E., Celona, B., Venereau, E., Apuzzo, T., De, M.F., Pedotti, M., Bachi, A. *et al.* (2012) HMGB1 promotes recruitment of inflammatory cells to damaged tissues by forming a complex with CXCL12 and signaling via CXCR4. *J. Exp. Med.*, **209**, 551–563.
53. Tang, D., Billiar, T.R. and Lotze, M.T. (2012) A Janus tale of two active high mobility group box 1 (HMGB1) redox states. *Mol. Med.*, **18**, 1360–1362.
54. Vidal, B., Serrano, A.L., Tjwa, M., Suelves, M., Ardite, E., De Mori, R., Baeza-Raja, B., Martínez de Lagrán, M., Lafuste, P., Ruiz-Bonilla, V. *et al.* (2008) Fibrinogen drives dystrophic muscle fibrosis via a TGFbeta/alternative macrophage activation pathway. *Genes Dev.*, **22**, 1747–1752.
55. Charan, R.A., Niizawa, G., Nakai, H. and Clemens, P.R. (2013) Adeno-associated virus serotype 8 (AAV8) delivery of recombinant A20 to skeletal muscle reduces pathological activation of nuclear factor (NF)-kappaB in muscle of mdx mice. *Mol. Med.*, **18**, 1527–1535.
56. Amenta, A.R., Yilmaz, A., Bogdanovich, S., McKechnie, B.A., Abedi, M., Khurana, T.S. and Fallon, J.R. (2011) Biglycan recruits utrophin to the sarcolemma and counters dystrophic pathology in mdx mice. *Proc. Natl. Acad. Sci. USA*, **108**, 762–767.
57. Henriques-Pons, A., Yu, Q., Rayavarapu, S., Cohen, T.V., Ampong, B., Cha, H.J., Jahnke, V., VanderMeulen, J., Wang, D., Wayne, J. *et al.* (2014) Role of Toll like receptors in the pathogenesis of dystrophin-deficient skeletal and heart muscle. *Hum. Mol. Genet.*, **23**, 2604–2617.

58. Uaesoontrachoon, K., Cha, H.-J., Ampong, B., Sali, A., Vandermeulen, J., Wei, B., Creeden, B., Huynh, T., Quinn, J., Tatem, K. *et al.* (2013) The effects of MyD88 deficiency on disease phenotype in dysferlin-deficient A/J mice: role of endogenous TLR ligands. *J. Pathol.*, **231**, 199–209.
59. Tu, J.H., He, Y.J., Chen, Y., Fan, L., Zhang, W., Tan, Z.R., Huang, Y.F., Guo, D., Hu, D.L., Wang, D. *et al.* (2010) Effect of glycyrrhizin on the activity of CYP3A enzyme in humans. *Eur. J. Clin. Pharmacol.*, **66**, 805–810.
60. Manns, M.P., Wedemeyer, H., Singer, A., Khomutjanskaja, N., Dienes, H.P., Roskams, T., Goldin, R., Hehnke, U. and Inoue, H. (2012) Glycyrrhizin in patients who failed previous interferon alpha-based therapies: biochemical and histological effects after 52 weeks. *J. Viral Hepat.*, **19**, 537–546.
61. Beastrom, N., Lu, H., Macke, A., Canan, B.D., Johnson, E.K., Penton, C.M., Kaspar, B.K., Rodino-Klapac, L.R., Zhou, L., Janssen, P.M.L. *et al.* (2011) mdx(^{5}cv) mice manifest more severe muscle dysfunction and diaphragm force deficits than do mdx Mice. *Am. J. Pathol.*, **179**, 2464–2474.
62. Briguet, A., Courdier-Fruh, I., Foster, M., Meier, T. and Magyar, J.P. (2004) Histological parameters for the quantitative assessment of muscular dystrophy in the mdx-mouse. *Neuromuscul. Disord.*, **14**, 675–682.
63. Schneider, C.A., Rasband, W.S. and Eliceiri, K.W. (2012) NIH Image to ImageJ: 25 years of image analysis. *Nat. Methods*, **9**, 671–675.
64. Straub, V., Rafael, J.A., Chamberlain, J.S. and Campbell, K.P. (1997) Animal models for muscular dystrophy show different patterns of sarcolemmal disruption. *J. Cell Biol.*, **139**, 375–385.
65. Divangahi, M., Demoule, A., Danialou, G., Yahiaoui, L., Bao, W., Xing, Z. and Petrof, B.J. (2007) Impact of IL-10 on diaphragmatic cytokine expression and contractility during Pseudomonas Infection. *Am. J. Respir. Cell Mol. Biol.*, **36**, 504–512.
66. Stout, R.D., Jiang, C., Matta, B., Tietzel, I., Watkins, S.K. and Suttles, J. (2005) Macrophages sequentially change their functional phenotype in response to changes in microenvironmental influences. *J. Immunol.*, **175**, 342–349.
67. Agarwal, R., Wang, Z.Y. and Mukhtar, H. (1991) Inhibition of mouse skin tumor-initiating activity of DMBA by chronic oral feeding of glycyrrhizin in drinking water. *Nutr. Cancer*, **15**, 187–193.